ARTICLE

fib WILEY

Theoretical and experimental investigation of the time-dependent relaxation rates of GFRP and BFRP reinforcement bars

Dominik Hiesch | **Tilo Proske** | **Carl-Alexander Graubner** |
Lukas Bujotzek | **Redouan El Ghadioui**

TU Darmstadt, Institute of Concrete and Masonry Structures, Darmstadt, Germany

Correspondence
Dominik Hiesch, TU Darmstadt, Institute of Concrete and Masonry Structures, Franziska-Braun-Str. 3, 64287 Darmstadt, Germany.
Email: hiesch@massivbau.tu-darmstadt.de

Abstract

Cracked concrete members with fiber-reinforced polymer (FRP) reinforcement generally suffer from increased deflections compared to steel-reinforced members due to FRP reinforcements' lower modulus of elasticity. An approach to counteract this problem can be the prestressing of the FRP reinforcement, which can significantly reduce member deflections. However, time-dependent prestress losses occur due creep and shrinkage of the concrete and relaxation of the prestressing tendons. Within the first part of this article, mathematical approaches to determine relaxation rates from creep tests are introduced. Subsequently, short-term and long-term tensile tests under sustained load on glass and basalt FRP reinforcement bars are presented. Based on the experimental data and the mathematical model, relaxation rates for the investigated specimens are derived. In addition, using an approach based on logarithmic extrapolation, the relaxation rates at 1 million hours (end of service life) are calculated, and the experimentally determined residual tensile properties are evaluated.

KEYWORDS
concrete, creep, fiber-reinforced polymer, FRP, prestress, relaxation

1 | INTRODUCTION

Due to corrosion of the steel reinforcement, concrete structures with steel reinforcement often do not achieve the service lives demanded by design codes.[1] Thus, those

structures have to be repaired or replaced prematurely. To address this issue, a wide variety of investigations on fiber-reinforced polymer (FRP) reinforcement have been carried out, including past and current research projects, focusing on different types of reinforcement fibers such as carbon,[2,3] basalt,[4,5] or glass[6,7] and the work of standards committees and general literature.[8–10] Due to favorable properties like their high tensile strength, low weight, and high resistance against corrosion, FRP reinforcement can be a viable alternative for regular steel

---

reinforcement, especially in highly corrosive environments. When using FRP reinforcement, the lower modulus of elasticity compared to steel reinforcement has to be considered, resulting in increased member deflections in State II. In addition, a smaller reinforcement area is required in the ultimate limit state due to the high tensile strength, further aggravating the deflection problem. As a result, the design of FRP reinforced concrete members is generally determined by their serviceability instead of their maximum load-bearing capacity. To counteract this issue, the research on prestressed FRP reinforcement was intensified (e.g., Nanni and colleagues[10–12]). The prestressing force within the FRP tendon induces compressive stress in the adjacent concrete, increasing the member's cracking moment. Therefore, the transition from State I to State II occurs at a higher load level. Due to the higher member stiffness at the unaltered service load level, the corresponding member deflection in the serviceability limit state is reduced. However, due to creep and shrinkage of the concrete and relaxation of the prestressing tendons, time-dependent prestress losses occur, reducing the effect of the initial prestressing over time. When changing the material of the prestressing tendon, the modulus of elasticity and the relaxation properties of the prestressing tendon determine the changes of the prestress losses; see Przygocka et al.[13] for an overview of this subject. Generally, prestress losses in concrete members with prestressed FRP reinforcement tend to be smaller due to their lower modulus of elasticity compared to prestressing steel.

However, FRP reinforcement bars also have a pronounced relaxation potential due to their composition. FRP are defined as a composite material consisting of fibers and a polymer matrix.[14] According to Hull and Clyne,[15] ACI 440.4R-04,[16] and Dolan et al.,[17] the relaxation of FRP reinforcement bars is composed of two main components. The first component is the relaxation of the polymer matrix, resulting from a stress redistribution from the matrix onto the stiffer fibers. According to Dolan et al.,[17] the scale of this relaxation component can be estimated by multiplication of the ratio of the moduli of elasticity of the matrix and the fibers E_m/E_f and the matrix volume content $V_m = (1 - V_f)$. Considering values of $E_m \approx 3500$–5000 N/mm^2 for vinyl ester and epoxy resin respectively and values of $E_f \approx 80,000$ and $200,000$ N/mm^2 for glass/basalt and carbon fibers, see Ehrenstein,[14] as well as matrix volume contents of $V_m \approx 0.25$–0.5, see Youssef et al.,[18] the matrix relaxation causes stress losses of approximately 1.1%–3.1% (glass fiber-reinforced polymer [GFRP]/basalt fiber-reinforced polymer [BFRP]) and 0.4%–1.3% (CFRP) of the initial stress.

The second component is the relaxation of the fibers, depending on the fiber material. According to Dolan

et al.[17] and Ascione et al.[19] carbon and glass fibers are not subject to relaxation. This statement can be extended to basalt fibers, since their mineral composition is very similar to that of glass fibers. Aramid fibers however, undergo a significant relaxation of up to 18% on the initial stress across a service life of 100 years according to Dolan et al.[17]

This paper deals with the FRP relaxation behavior, which is reviewed based on existing tests and by comparing two different methods of computing the relaxation rate of FRP reinforcement. Then, the short-term material properties of two types of FRP reinforcement (GFRP and BFRP) are experimentally determined. Based on these results, long-term tensile tests on these reinforcements are conducted to experimentally determine the relaxation rates over a period of 1000 h. In addition, a calculative approach to extrapolate the relaxation rate over the entire service life is presented and the residual tensile properties of the FRP reinforcements after the long-term test are evaluated.

1.1 | Research significance

Based on international guidelines like ACI 440.4R-04[16] or fib bulletin 40,[20] it is not permitted to prestress GFRP and BFRP reinforcement, while CSA-S6-14[21] permits prestressing of GFRP reinforcement of up to 25% of the ultimate tensile strength. The research in this paper assesses the time-dependent properties of GFRP and BFRP reinforcement based on load levels of up to 50% of the ultimate tensile strength (one sample was subjected to a sustained load of 70% of its ultimate tensile strength) over a period of 1000 h. Based on the results of this work, relaxation losses, which are an integral component of the overall prestress losses, can be estimated in order to design safe concrete structures with prestressed GFRP and BFRP reinforcement that reach the requested service lives of up to 100 years.[22]

2 | FRP RELAXATION BEHAVIOR AND REVIEW OF EXISTING TESTS

2.1 | General

As mentioned above, the relaxation of prestressed FRP reinforcement is a highly time-dependent property that can vary greatly depending on the material composition and the initial stress level.[8] By definition, relaxation describes a progressive decrease of stress over time under a constant strain.[23] Equation (1) expresses the corresponding relaxation rate ψ at any given time t.

$$\psi(t,t_0) = \frac{\Delta\sigma(t,t_0)}{\sigma_0} = \frac{\sigma_0 - \sigma(t)}{\sigma_0}, \qquad (1)$$

where $\psi(t,t_0)$ is relaxation rate depending on time t, $\Delta\sigma(t,t_0)$ is time-dependent stress decrease, $\sigma(t)$ is stress depending on time t, and σ_0 is initial stress.

To experimentally determine this relaxation rate for a given material, a constant strain must be applied to a specimen while the stress is continuously recorded over time. Such relaxation tests are somewhat difficult to set up and to maintain over an extended period, since anchorage slippage influences the strain application over time. Researchers often examine the creep behavior of the specimens instead, because according to Trost,[23] both phenomena are closely related to one another and creep tests in a force-controlled setup are easier to carry out and maintain. Creep describes the progressive increase of strain over time under constant stress.[23] The corresponding creep rate φ at any time t can be expressed according to Equation (2).

$$\varphi(t,t_0) = \frac{\Delta\varepsilon(t,t_0)}{\varepsilon_0} = \frac{\varepsilon(t) - \varepsilon_0}{\varepsilon_0}, \qquad (2)$$

where $\varphi(t,t_0)$ is creep rate depending on time t and the time of loading t_0, $\Delta\varepsilon(t,t_0)$ is time-dependent strain increase, $\varepsilon(t)$ is strain depending on time t, and ε_0 is initial strain.

Stress and strain, and therefore creep and relaxation, are directly connected by a material's modulus of elasticity $E(t)$. It is possible to calculate a material's relaxation rate when knowing its creep rate and vice versa. Trost states that for materials like concrete and steel, it can be assumed that a given value of the modulus of elasticity does not significantly change over time, even when the material is subjected to constant stress or strain, giving $E(t) = E_0$. This assumption is extended to FRPs in Sections 2.2–2.4 and later validated in Section 4.4.

2.2 | Approach by Trost

To mathematically connect the creep and relaxation phenomena, Trost[24] derived a relaxation coefficient ρ from the differential equation of time-invariant strain, see also Trost,[23] based on the material properties of concrete. This relaxation coefficient considers the decreasing relaxation intensity due to the aging of concrete, which is the reason it is often called the aging coefficient. It depends on the progression of stress over time as well as the corresponding creep rates and leads to Equation (3):

$$\frac{\sigma(t)}{\sigma_0} = 1 - \frac{\varphi(t,t_0)}{1 + \rho \times \varphi(t,t_0)}, \qquad (3)$$

where $\varphi(t,t_0)$ is creep rate depending on time t and the time of loading t_0 and ρ is relaxation coefficient (aging coefficient).

By merging Equations (1) and (3), Trost converts creep rates $\varphi(t,t_0)$ to relaxation rates $\psi(t,t_0)$ utilizing Equation (4).

$$\psi(t,t_0) = \frac{\varphi(t,t_0)}{1 + \rho \times \varphi(t,t_0)}. \qquad (4)$$

According to Trost,[23,24] the value of ρ can theoretically vary between $\rho_{\min} = 0.5$ (linear growth of the relaxation losses over time) and $\rho_{\max} = 1.0$ (a constant value of the relaxation losses over time with all losses occurring immediately at the time of loading). However, based on his empirical study of a wide range of test results on concrete specimens, Trost found that the relaxation coefficient can be taken as $\rho = 0.8$, leading to sufficiently precise results in general cases regarding concrete structures. Even though the derivation and calibration of the relaxation coefficient ρ are entirely based on concrete, the tendency of decreasing relaxation intensity can also be expected from other time-variant materials, such as FRPs. However, the applicability of Equation (4) and the value of $\rho = 0.8$ have to be reviewed for FRPs. Therefore, a second approach based on an iterative conversion of creep rates to relaxation rates, according to Shi et al.,[25] is presented in the following.

2.3 | Approach by Shi et al.

The experimental results of long-term relaxation tests with BFRP tendons by Shi et al.[25] showed that the viscoelastic strain ε_ν is proportional to the square of the stress level. Based on this observation, Shi et al.[25] derived Equation (5) to iteratively calculate the remaining time-dependent stress in the specimen based on creep test results. Accordingly, the recorded strain increment $\Delta\varepsilon_{\nu,\exp}$ from the creep test is adjusted by considering the decreasing stress level in the specimen, which is taken as proportional to the square of the stress ratio. As in Trost's approach, the modulus of elasticity is assumed to be constant $E(t) = E_0$.

$$\sigma_n = \sigma_{n-1} - E_0 \times \Delta\varepsilon_{\nu,\exp} \times (\sigma_{n-1}/\sigma_0)^2, \qquad (5)$$

where σ_n is stress at calculation step n, σ_{n-1} is stress at calculation step $n-1$, and $\Delta\varepsilon_{\nu,\exp}$ is recorded strain increment between the time steps t_n and t_{n-1}.

TABLE 1 Overview of creep tests on FRP reinforcement bars (from literature and this research).

Source	Test ID	Material	V_f (%)	Ø (mm)	$\sigma_0/f_{t,m}$ (%)	E_{calc} (N/mm²)	Duration (h)	φ_{exp} (%)	ψ_{calc} (%) Shi et al.	Trost	ψ_{Trost}/ψ_{Shi} (−)
Youssef and Benmokrane	1	Glass, vinyl ester	57	9.5	12.4	46,774	10,000	4.11	4.00	3.98	1.00
	2				12.4	46,691		7.76	7.40	7.31	0.99
	3				12.6	46,663		7.20	6.93	6.81	0.98
	4				14.8	46,760		8.84	8.52	8.26	0.97
	5				20.9	46,859		1.21	1.21	1.20	0.99
	6				28.8	46,803		3.79	3.71	3.68	0.99
	7	Glass, vinyl ester	65	12.7	16.2	49,443	10,000	2.01	1.99	1.98	0.99
	8				16.2	49,659		3.64	3.56	3.54	0.99
	9				16.0	49,596		4.08	3.98	3.96	0.99
	10				24.3	49,626		5.30	5.21	5.09	0.98
	11				25.1	49,534		12.03	11.29	10.98	0.97
	12				25.9	49,620		6.31	6.08	6.01	0.99
	13				25.6	49,474	3000	1.52	1.51	1.50	0.99
	14	Glass, vinyl ester	67	15.9	14.1	42,272	10,000	5.81	5.62	5.55	0.99
	15				15.7	42,107		4.23	4.12	4.09	0.99
	16				15.4	42,303		4.92	4.80	4.73	0.99
	17				14.1	42,238		8.29	7.94	7.77	0.98
	18				37.3	42,190		3.18	3.11	3.10	1.00
	19				30.9	42,216		8.58	8.24	8.03	0.97
	20				29.1	42,167		6.57	6.47	6.24	0.96
	21				29.4	42,177		6.16	5.93	5.87	0.99
	22	Glass, vinyl ester	51	9.5	10.5	44,791	10,000	1.70	1.68	1.68	1.00
	23				11.4	44,842		2.52	2.53	2.47	0.98
	24				37.6	44,821		11.79	11.46	10.77	0.94
	25				29.1	44,811		2.01	2.00	1.98	0.99
	26				48.7	44,774		2.44	2.43	2.40	0.99
	27				30.3	44,801		5.50	5.36	5.27	0.98
	28	Glass, vinyl ester	58	15.9	15.4	40,751	10,000	15.68	14.77	13.93	0.94
	29				14.8	40,690		9.69	9.28	8.99	0.97
	30				19.0	40,681		15.67	14.73	13.92	0.95

(Continues)

TABLE 1 (Continued)

Source	Test ID	Material	V_f (%)	Ø (mm)	$\sigma_0/f_{t,m}$ (%)	E_{calc} (N/mm²)	Duration (h)	φ_{exp} (%)	ψ_{calc} (%) Shi et al.	ψ_{calc} (%) Trost	ψ_{Trost}/ψ_{Shi} (−)
	31				17.1	40,598		11.37	10.88	10.42	0.96
	32				37.6	42,385		11.79	11.46	10.77	0.94
	33				29.1	42,375		2.01	2.00	1.98	0.99
	34				48.7	42,341		2.44	2.43	2.40	0.99
	35				30.3	42,366		5.50	5.36	5.27	0.98
	36	Glass, vinyl ester	75	12.0	12.9	65,759	10,000	2.21	2.17	2.17	1.00
	37				16.0	66,120		3.22	3.17	3.14	0.99
	38				13.0	66,054		2.59	2.56	2.54	0.99
	39				20.0	66,104		4.71	4.58	4.54	0.99
	40				17.2	65,902		1.66	1.68	1.64	0.98
	41				19.1	65,830		5.65	5.55	5.40	0.97
Sayed-Ahmed et al.	42	Glass, vinyl ester	–	10.0	21.0	75,127	1670	5.81	5.55	5.55	1.00
	43				22.0	72,571		3.90	3.78	3.78	1.00
	44				20.0	73,357		6.86	6.53	6.50	1.00
	45				40.0	74,982		6.55	6.25	6.22	1.00
	46				40.0	73,094		8.54	8.01	8.00	1.00
	47				41.0	73,858		11.17	10.23	10.25	1.00
Shi et al. and Wang et al.	48	Basalt, vinyl ester	60	6.0	50.0	46,211	1000	2.04	2.02	2.01	1.00
	49					46,665		4.27	4.18	4.13	0.99
	50					46,082		4.42	4.30	4.27	0.99
	51				60.0	46,490		2.25	2.23	2.21	0.99
	52					45,670		3.70	3.62	3.59	0.99
	53					45,976		5.15	5.06	4.95	0.98
Yang et al.	54	Carbon, epoxy	65	8.0	69.0	147,132	1000	1.12	1.11	1.11	1.00
	55					147,365		1.10	1.09	1.09	1.00
	56					147,540		1.03	1.02	1.02	1.00
	57				76.0	146,060		1.11	1.10	1.10	1.00
	58					146,047		1.15	1.14	1.14	1.00
	59					146,399		1.06	1.05	1.05	1.00
	60				85.0	150,397		1.19	1.18	1.18	1.00

TABLE 1 (Continued)

| Source	Test ID	Material	V_f (%)	Ø (mm)	$\sigma_0/f_{t,m}$ (%)	E_{calc} (N/mm²)	Duration (h)	φ_{exp} (%)	ψ_{calc} (%) Shi et al.	ψ_{calc} (%) Trost	ψ_{Trost}/ψ_{Shi} (−)
	61					142,869		1.16	1.15	1.15	1.00
	62					148,020		1.13	1.12	1.12	1.00
Hiesch et al.	63	Glass, vinyl ester	75	8.0	25.0	47,318	1000	2.04	2.01	2.00	1.00
	64					47,722		1.79	1.77	1.76	0.99
	65					51,782		3.09	3.01	3.01	1.00
	66					50,685		3.94	3.83	3.82	1.00
	67					47,302		1.57	1.55	1.55	1.00
	68				40.0	49,500		3.93	3.81	3.81	1.00
	69					44,825		4.10	3.97	3.97	1.00
	70					47,678		2.26	2.22	2.22	1.00
	71			12.0	20.0	50,290		3.67	3.57	3.57	1.00
	72					50,061		2.65	2.59	2.60	1.00
	73	Basalt, epoxy	77	8.0	40.0	43,588		3.39	3.30	3.30	1.00
	74					39,416		4.09	3.95	3.96	1.00
	75				50.0	42,368		6.10	5.80	5.82	1.00
	76					46,100		2.70	2.64	2.64	1.00
	77					46,150		4.15	4.02	4.02	1.00
	78			10.0	40.0	42,296		2.50	2.45	2.45	1.00
	79					43,573		4.08	3.93	3.95	1.01
	80				70.0	45,935		4.06	3.91	3.93	1.01
									Mean value (−)		0.99
									Coefficient of variation (%)		1.5
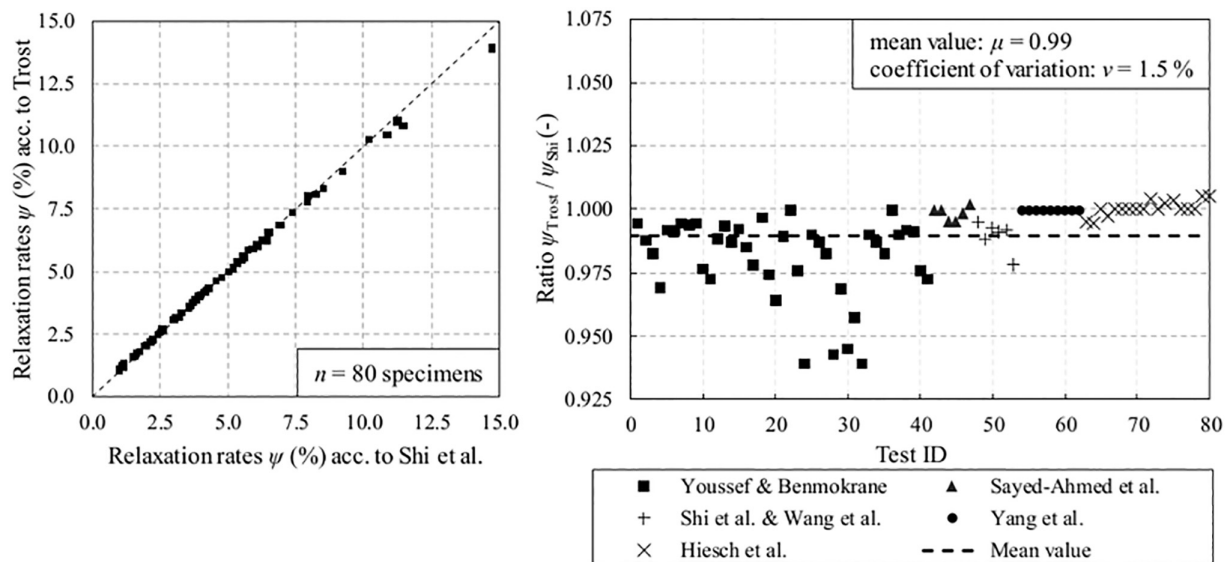
FIGURE 1 Comparison of relaxation rates according to Trost[24] and Shi et al.[25]

Finally, the relaxation rate is calculated using Equation (1) with $\sigma(t)$ being the calculated remaining stress after the final calculation step according to Equation (5). For multiple creep tests conducted by Wang et al.,[26] Shi et al.[25] showed that the relaxation rates calculated in this manner are in good agreement with the experimentally determined relaxation rates from actual relaxation tests on the same type of FRP reinforcement.

2.4 | Review of existing creep tests and comparison of the approaches by Trost and Shi et al.

While the two approaches by Trost and Shi et al. are based on the same mechanical principles, see Equation (1), the approach by Trost is easier to handle due to the empirically determined relaxation coefficient $\rho = 0.8$. In contrast, the method by Shi et al. is based on an extensive iterative calculation. To verify the applicability of Trost's relaxation coefficient for FRP reinforcement, a database of creep tests on FRP reinforcement bars, shown in Table 1, is compiled. The relaxation rate for each specimen is calculated using both methods. When comparing the relaxation rates of the 80 tests specified in Table 1 and shown in Figure 1, an excellent agreement with a mean ratio of $\psi_{\text{Trost}}/\psi_{\text{Shi}} \approx 0.99$ between the two approaches can be found.

In addition, the right part of Figure 1 shows the ratio of the relaxation rates calculated with the two approaches. The results are separated into five different clusters, regarding the various testing facilities and material combinations of Youssef and Benmokrane,[18] Sayed-

Ahmed et al.,[27] Yang et al.,[28] Shi et al.,[25] and Wang et al.[26] and the authors of this paper, see also Table 1. The differences between the two approaches are generally minor. Still, within the sample of Youssef and Benmokrane, the most significant differences between the two approaches can be observed, with ratios of $\psi_{\text{Trost}}/\psi_{\text{Shi}} \approx 0.94$ for some specimens. When comparing these tests with the ones with ratios of $\psi_{\text{Trost}}/\psi_{\text{Shi}} \approx 1.00$, no correlation between the rate $\psi_{\text{Trost}}/\psi_{\text{Shi}}$ and the material combination, bar diameter and load level can be found. However, when looking at the calculation results for authors' tests or the tests of Yang et al., the best agreement between the two approaches can be found. This difference is mainly attributed to the resolution of the underlying creep test data. The iterative approach of Shi et al. depends on the course of the creep strain over time. Therefore, the method's accuracy is dependent on the resolution of the measured creep strain. For the authors' tests as well as the tests of Yang et al., the given creep values are tightly spaced (≥ 25 data points within the first 1000 h), leading to very good accordance between the two approaches. Conversely, for the tests of Youssef and Benmokrane, the creep values are only available at three points (1000, 3000, and 10,000 h), omitting the critical period of early creep within the first 1000 h. Therefore, the accuracy of the iterative calculation is reduced, resulting in increased deviations between the two approaches, with the iteratively calculated relaxation rates being generally bigger than the relaxation rates according to Trost. It is observed that the iterative approach by Shi et al. tends to converge to the value, according to Trost, when taking a more extensive number of data points into account. Overall, the differences between the two

FIGURE 2 Investigated GFRP and BFRP reinforcement bars.

approaches remain small for all investigated cases and both computational methods tend to converge toward the same value. This illustrates that by using the approach by Trost with the associated value of $\rho = 0.8$, the relaxation rates of FRP reinforcement bars can be calculated based on creep test results sufficiently precise. Therefore, the experimental program of this research will be based on long-term creep tests, shown in Section 4. Subsequently, the experimentally determined creep rates will be transformed into relaxation rates using Equation (4).

3 | SHORT-TERM TENSILE TESTS

3.1 | Materials

In this study, two types of FRP reinforcement bars, which are shown in Figure 2, are investigated. The first type, a GFRP reinforcement with a grooved surface, is composed of ECR-glass fibers and vinyl ester resin with a fiber volume content of $V_{f,G} = 75\%$, according to the manufacturer. Specimens with the nominal diameters of $\varnothing_{nom} = 8$ and 12 mm have been investigated, whose effective cross-sectional areas are $A_{eff,G,8mm} = 60.94$ mm^2 and $A_{eff,G,12mm} = 137.12$ mm^2, respectively. The second type, a BFRP reinforcement with a helically wrapped and sand-coated surface, is composed of basalt fibers and epoxy resin with a fiber volume content of $V_{f,B} = 77\%$, according to its manufacturer. Reinforcement bars with nominal diameters of $\varnothing_{nom} = 8$ and 10 mm and effective cross-sectional areas of $A_{eff,B,8mm} = 43.10$ mm^2 and $A_{eff,B,10mm} = 69.27$ mm^2 have been tested. The stated effective cross-sectional areas of all tested reinforcements were determined according to ASTM D7205/D7205M-06[29] by immersion weighing of each reinforcement type and diameter.

3.2 | Test-setup and specimen preparation

The average short-term tensile properties of each type of FRP bar were determined following ASTM D7205/D7205M-06[29] by tensile tests until failure in the testing

FIGURE 3 Short-term tensile test on a GFRP reinforcement bar in a universal testing rig.

rig shown in Figure 3. The force was measured by the testing rigs load cell (range up to 400 kN, precision ± 0.2 kN). The strains needed to calculate the modulus of elasticity were measured with electronic DD1 strain transducers (upper device on the specimen in Figure 3) with a stroke length of ± 2.5 mm and a precision of ± 0.0025 mm.

The anchorage described in ASTM D7205/D7205M-06[29] is recommended for monotonic tensile tests and creep or relaxation tests with a maximum load of 400 kN. Thus, it is suitable for all tests carried out within the framework of this research. The ends of each specimen were centered in steel tubes and filled with an expansive cement grout, see Figure 4. The free lengths have been calculated to $L_{\varnothing 8mm} = 380$ mm, $L_{\varnothing 10mm} = 400$ mm, and
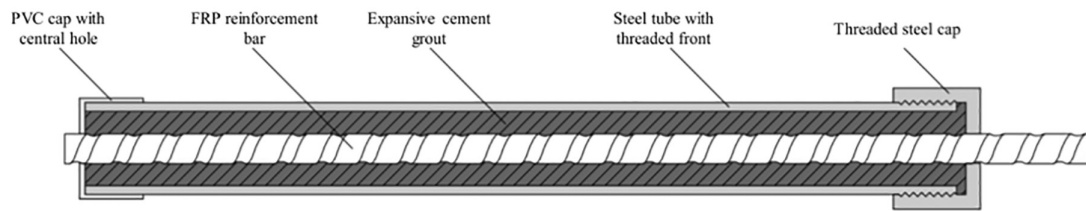
FIGURE 4 Schematic drawing of the anchorage used following ASTM D7205/D7205M-06.[29]

TABLE 2 Material properties of the investigated reinforcement bars.

Reinforcement	Type	V_f (%)	$\varnothing_{nom}$ (mm)	A_{eff} (mm^2)	$F_{t,m}$ (kN)	$f_{t,m}$ (N/mm^2)	E_m (N/mm^2)	$\varepsilon_{u,m}$ (‰)
GFRP Bars	Schöck Combar	75	8	60.94	70.8 ($\pm$3.3)	1161 ($\pm$54)	48,434 ($\pm$1889)	24.03 ($\pm$1.67)
			12	137.12	163.9 ($\pm$5.1)	1195 ($\pm$37)	49,757 ($\pm$546)	24.02 ($\pm$0.62)
BFRP Bars	DBF Basalt Rebar	77	8	43.10	41.2 ($\pm$0.5)	955 ($\pm$11)	47,611 ($\pm$1085)	20.06 ($\pm$0.23)
			10	69.27	65.8 ($\pm$2.2)	950 ($\pm$32)	42,846 ($\pm$1514)	22.20 ($\pm$1.31)

FIGURE 5 Typical failure mode of a GFRP reinforcement bar after reaching the tensile strength.

$L_{\varnothing 12mm}$ = 480 mm, according to ASTM D7205/D7205M-06.[29]

3.3 | Results and discussion

The average short-term tensile properties (the ultimate tensile load $F_{t,m}$, the tensile strength $f_{t,m}$, the modulus of elasticity E_m and the ultimate strain $\varepsilon_{u,m}$), as well as the corresponding standard deviations (in brackets) based on a sample size of up to 10 specimens each, can be taken from Table 2. Note that the tensile strength and modulus of elasticity are calculated using the effective cross-sectional area of the specimens A_{eff} given above. These short-term tensile properties are being used as reference values for the long-term tensile tests in Section 4, especially for determining the sustained load levels in the specimens of the long-term tests.

All specimens showed the typical linear-elastic behavior and a dispersed broom-like failure within the free length, shown in Figure 5. None of the tested specimens failed in or around the anchorage region, indicating the suitability of this type of anchorage for tensile tests on the FRP reinforcement bars within this research.

4 | LONG-TERM TENSILE TESTS

4.1 | Test-setup and preparation

To monitor potential changes of the mechanical properties due to sustained long-term loads, the stress–strain relationship of each FRP reinforcement bar intended for the creep tests was determined before and after the long-term test in the same testing rig shown in Figure 2. After preparation, each specimen was loaded with the intended load level for the long-term test. To define the intended load levels for the long-term tensile tests, international guidelines as well as other research initiatives are being evaluated. The creep-rupture stress limit for GFRP reinforcement is set at around 20%–25% of the specimen's ultimate tensile strength, according to various international guidelines.[9,20,21,30] However, Rossini et al.[31] showed that the guaranteed creep-rupture strength of different GFRP reinforcement bars, is equal to around 40% of their ultimate tensile strength. Therefore, the intended stress levels in the long-term tensile tests are based on the creep-rupture stress limits given be the guidelines (0.2–$0.25 \times f_{t,m}$) and according to Rossini et al.[31] ($0.4 \times f_{t,m}$). For the specimens V1–V5 and V9–V10 load levels of $\sigma_0/f_{t,m} = 0.25$ and $\sigma_0/f_{t,m} = 0.2$ and for the specimens V6–V8 as well as V11–V12 and V16–V17 load levels of $\sigma_0/f_{t,m} = 0.4$ were chosen. In addition, the specimens V13–V15 and the specimen V18 were subjected to higher load levels of $\sigma_0/f_{t,m} = 0.5$ and $\sigma_0/f_{t,m} = 0.7$, respectively, in order to assess possible effects of increased load levels, as stress levels of around 70% of the mean ultimate tensile strength did not lead to creep-rupture failure within the period of 1000 h in the tests of Rossini et al.[31]

FIGURE 6 Schematic drawing of the used strain measuring device.
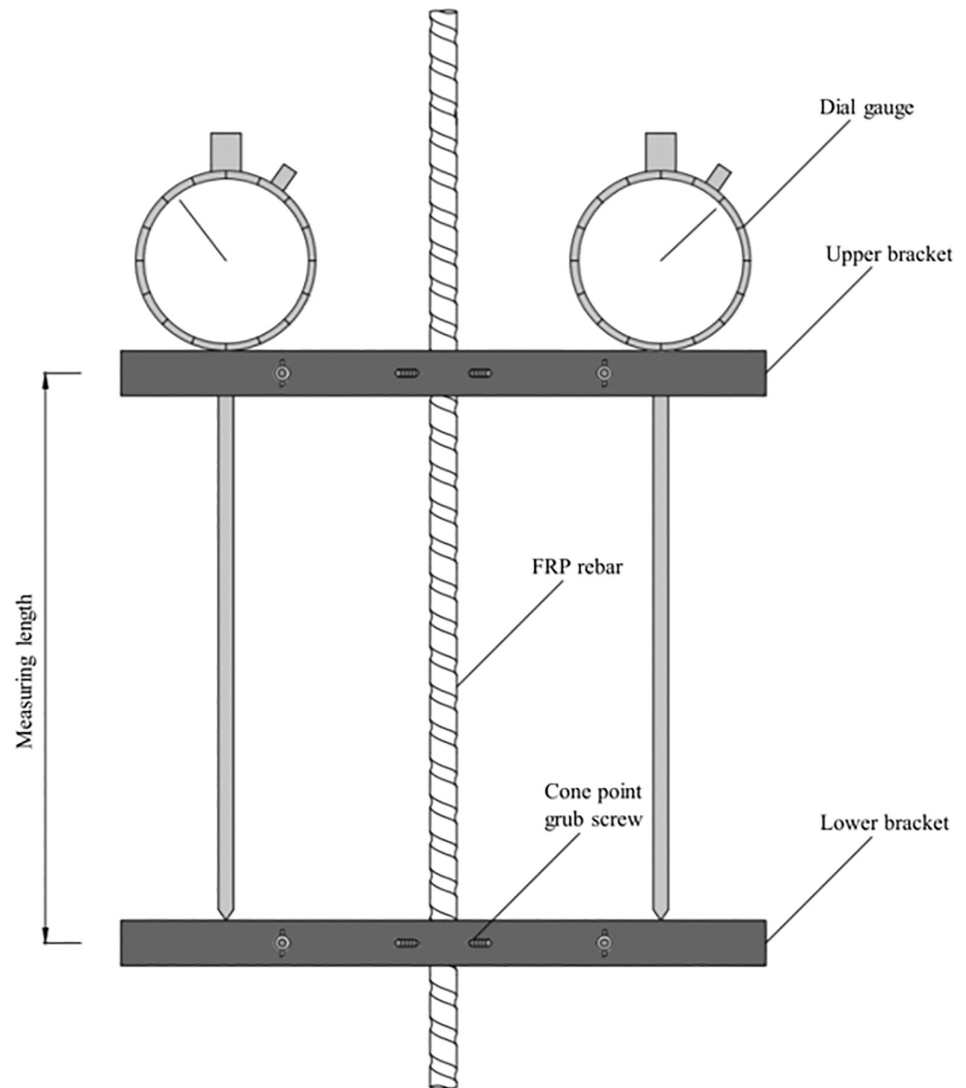
To measure the strain and the related changes over time, the specimens were fitted with a strain measurement device consisting of two dial gauges (stroke length 10 mm, precision ±0.01 mm) and two brackets fitted to the specimens, as shown in Figure 6. The precision of this device was evaluated with control measurements with the DD1 strain transducers, see Section 3.2, resulting in differences of less than 1.5% between the two devices, proving the suitability of this strain measurement device. Throughout the first 24 h of each test, the strain is measured and recorded continuously with the DD1 strain transducers and at several points additionally with the dial gauges for comparison. Afterwards, the strain was measured and recorded with the dial gauges every 24 h for another 4–6 days. Subsequently a measurement was taken at least every 120 h, in accordance with ACI 440.3R-12.[32] The exact data acquisition points beyond the continuous measurement (after 24 h) are highlighted in results in Figure 8.

The test frame for the long-term tests is shown in Figure 7. The applied load was magnified using the lever principle by a factor between 10 and 12, depending on the exact frame layout. The front brackets of the frame, where the test specimens are installed, are hinged in an articulated manner allowing for a self-aligning specimen installation. This way, the axial load introduction can be guaranteed, and the test specimens experience as little unplanned load eccentricity as possible.

The long-term tests were performed in a controlled environment with a temperature of $T = 21°C$ ($\pm1.5°C$) and a relative humidity of RH = 60% ($\pm5\%$).

4.2 | Results and discussion

As shown in Figure 7, the load is applied in a force-controlled manner, by attaching steel plates (weights) with slings to the upper beam of the test frame. In this
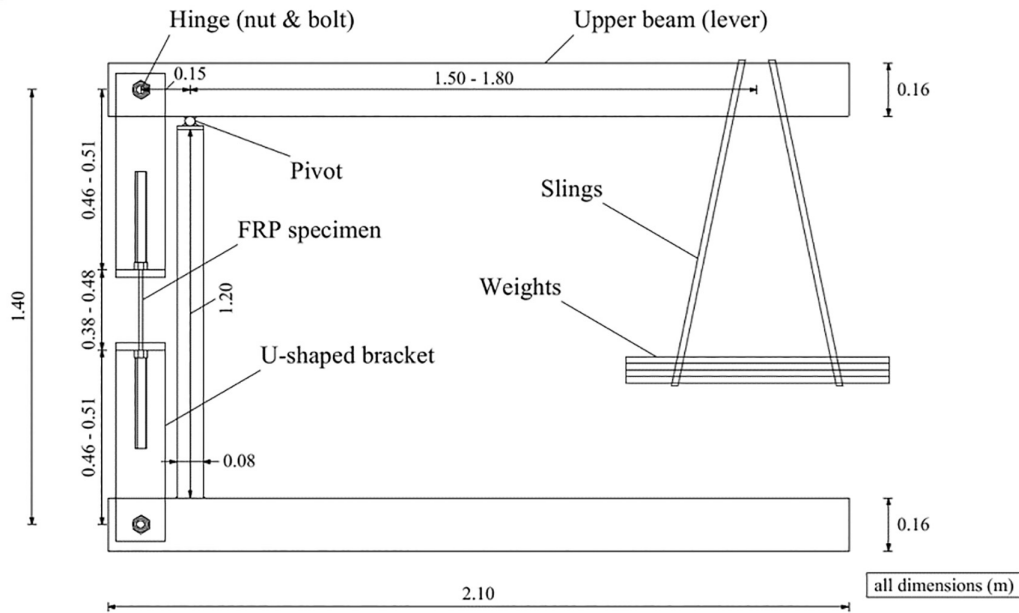
FIGURE 7 Schematic drawing of the long-term test frame setup.

TABLE 3 Measured creep rates and corresponding calculated relaxation rates.

Reinforcement	Specimen	$\varnothing_{nom}$ (mm)	$\sigma_0/f_{t,m}$ (%)	t (h)	φ (%)	ψ (%)
GFRP	V1	8	25	1000	2.04	2.00
	V2				1.79	1.76
	V3				3.09	3.01
	V4				3.94	3.82
	V5				1.57	1.55
	V6		40		3.93	3.81
	V7				4.10	3.97
	V8				2.26	2.22
	V9	12	20		3.67	3.57
	V10				2.65	2.60
BFRP	V11	8	40		3.39	3.30
	V12				4.09	3.96
	V13		50		6.10	5.82
	V14				2.70	2.64
	V15				4.15	4.02
	V16	10	40		2.50	2.45
	V17				4.08	3.95
	V18		70		4.06	3.93
GFRP—average				1000	2.90	2.83
BFRP—average					3.88	3.76

force-controlled setup, it could be guaranteed that the load remained constant over time. The resulting creep rates are directly transformed into relaxation rates using Equation (4) with a fixed relaxation coefficient of $\rho = 0.8$, as shown in Section 2. All 18 tests are conducted over 1000 h and are presented in Table 3 and Figure 8.
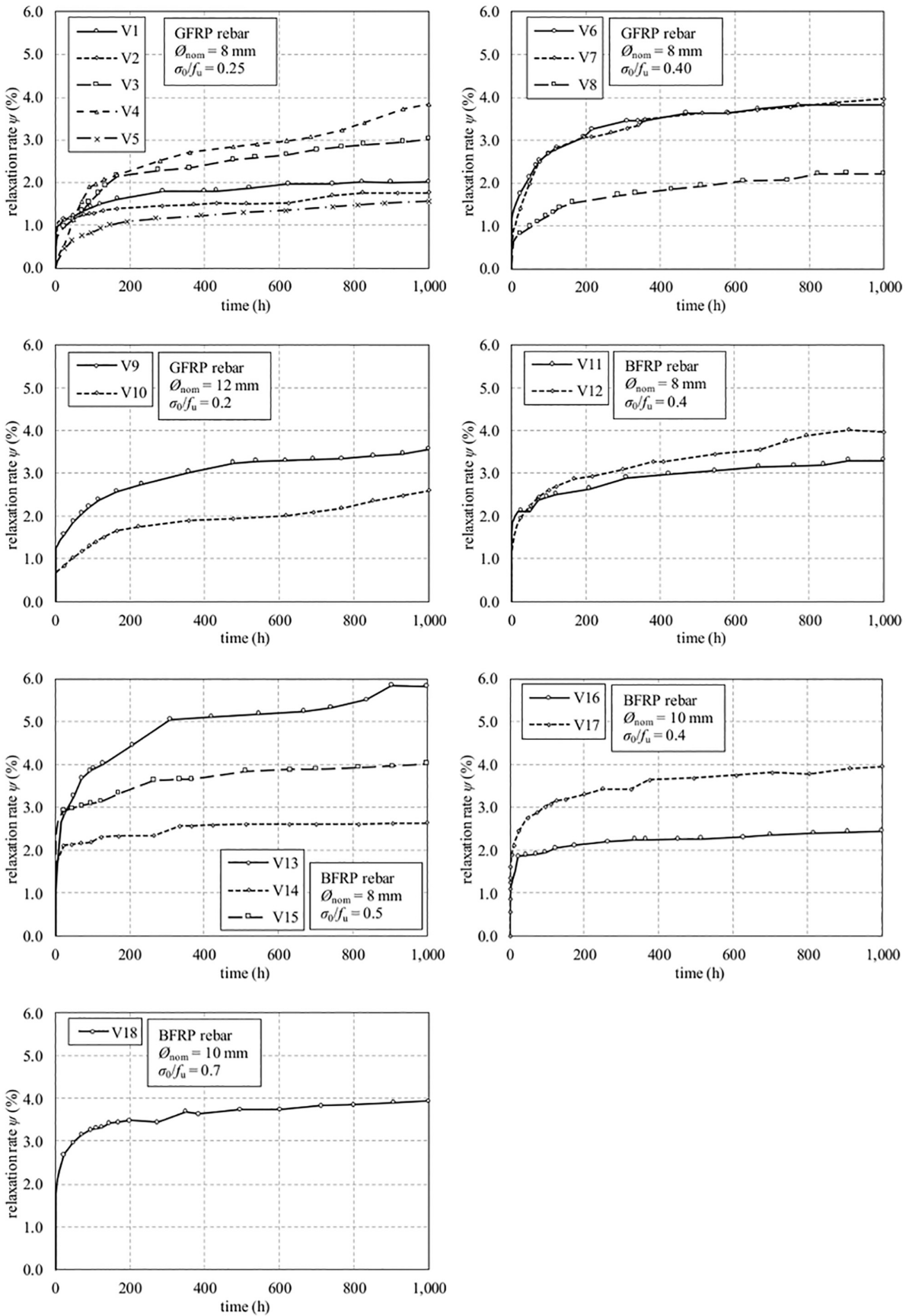
FIGURE 8   Relaxation rates over time for different load levels and reinforcement types.

The observed relaxation rates of specimens investigated up to 1000 h range from $\psi_{1000h} = 1.76\%$ to $\psi_{1000h} = 5.82\%$, with ranges of $1.55\% \leq \psi_{1000h,GFRP} \leq 3.97\%$ and $2.45\% \leq \psi_{1000h,BFRP} \leq 5.82\%$ for the GFRP and the BFRP specimens, respectively. Considering the experimental boundary conditions such as material combinations, load levels and test duration, this matches up well with other experimental results obtained from literature, see Table 1. When looking at the relaxation behavior of the specimens V1–V8, increased load levels ($\sigma_0/f_{t,m} = 0.4$ for specimens V6–V8 compared to $\sigma_0/f_{t,m} = 0.25$ for specimens V1–V5) do not result in significantly higher relaxation rates after 1000 h. This result can be explained by taking the mechanical background of FRP relaxation into account. According to *fib* Bulletin 40,[20] the predominant relaxation component is the matrix relaxation and the accompanying stress redistribution from the matrix to the fibers, mainly in the first days after loading. Since the relaxation rates are compared after 1000 h, when matrix relaxation is generally completed, relaxation rates mostly independent of the sustained load level are expected, as varying load levels mainly change the timeframe for the matrix relaxation. The same behavior can be observed for BFRP reinforcement bars with different load levels, when comparing specimens V11–V12 and V16–V17 ($\sigma_0/f_{t,m} = 0.4$) with V13–V15 ($\sigma_0/f_{t,m} = 0.5$) and V18 ($\sigma_0/f_{t,m} = 0.7$). Even though some specimens experience a little more (e.g., V13) or less relaxation (e.g., V16), the general behavior and average relaxation rates across different load levels are of comparable magnitude.

In addition, specimens of the same type but different bar diameter also show relaxation properties in comparable ranges. GFRP reinforcement bars with nominal diameters of $\varnothing_{nom} = 8$ mm and $\varnothing_{nom} = 12$ mm show average relaxation rates of $\psi_{1000h,G,8mm} \approx 2.8\%$ and $\psi_{1000h,G,12mm} \approx 3.1\%$, respectively. Comparable results can also be found for BFRP. The specimens with nominal diameters of $\varnothing_{nom} = 8$ mm and $\varnothing_{nom} = 10$ mm show average relaxation rates of $\psi_{1000h,B,8mm} \approx 3.9\%$ and $\psi_{1000h,G,12mm} \approx 3.5\%$, respectively. Due to the inherent and not insignificant scatter due to the nature of composite materials, illustrated by the coefficients of variation of $\nu_{\psi1000h,G} = 33\%$ and $\nu_{\psi1000h,B} = 28\%$, specific reasons for these differences between different diameters of the same bar type of $\Delta\psi_G = 0.3\%$ and $\Delta\psi_B = 0.4\%$ are not clearly to identify. However, the marginally more pronounced scattering of BFRP specimens can be attributed to a slight difference in manufacturing quality. The GFRP reinforcement appears very uniform, indicating a homogenous cross-section along the length of the reinforcement. For the BFRP reinforcement a small surplus of resin can be observed in some areas of the bar, while other areas show a slight lack of resin. This indicates that the fibers are not impregnated evenly along the length of the reinforcement, leading to small differences of the cross-sectional stress distributions along the length of the bar which can result in slightly increased scattering of the creep coefficients and relaxation rates.

Finally, as shown by the average values in Table 3, it can be stated that the investigated GFRP specimens tend to show lower relaxation rates ($\psi_{1000h,G,m} \approx 2.8\%$) compared to BFRP specimens ($\psi_{1000h,B,m} \approx 3.8\%$). Considering that the fiber volume contents are almost identical, see Table 2, this difference can be attributed to the difference of the elastic moduli of the ECR-glass and basalt fibers and the epoxy and vinyl ester resin matrices. With average values of $E_{f,G} \approx 80{,}000$ N/mm^2 and $E_{f,B} \approx 90{,}000$ N/mm^2 for the ECR-glass fibers and the basalt fibers as well as $E_{m,EP} \approx 4000$ N/mm^2 and $E_{m,VE} \approx 3400$ N/mm^2 for the epoxy and vinyl ester resins, according to Park[33] and *fib* Bulletin 40,[20] the modular ratio of the BFRP reinforcement (basalt + epoxy) is around 30% greater than that of the GFRP reinforcement (ECR-glass + vinyl ester). This leads to greater initial stress in the matrix of the BFRP specimens and thus to greater relaxation values due to stress redistribution. Since the modular ratio and the ratio of the average experimental relaxation rates are of comparable size, it can be assumed, that the relaxation due to stress redistribution from the matrix to the fibers is the main component of the relaxation of the examined reinforcement bars. In addition, the expected relaxation rates for CFRP reinforcement should be even smaller than those of the investigated GFRP reinforcement, given the comparably high modulus of elasticity of carbon fibers. The results from the literature, see Table 1, confirm this statement when considering the tests of Yang et al.,[28] whose CFRP specimens only showed relaxation rates of around $\psi_{CFRP,Yang} \approx 1\%$ even at high stress levels of up to 85% of their tensile strength.

4.3 | Prediction of the end-of-life relaxation rates

Based on the experimental relaxation rates of the FRP reinforcement bars across 1000 h, the progression of the relaxation rates until the end of the service life has to be calculated. According to Eurocode 0,[22] the service life of structural members is typically set at 50 years for general buildings or at 100 years for bridges. Since concrete members with prestressed FRP reinforcement can generally be used within both of these areas, it is reasonable to predict the relaxation rates of the FRP reinforcement for a time frame of at least 100 years. The time of 100 years equals 876,600 h, and with most formulae for determining the prestress losses of prestressed concrete members being

TABLE 4 Predicted long-term relaxation rates at t_∞.

Reinforcement	Specimen	$\varnothing_{nom}$ (mm)	$\sigma_0/f_{t,m}$ (%)	t_{exp} (h)	ψ_{1000h} (%)	a_{log} (−)	b_{log} (−)	R^2 (−)	ψ_∞ (Equation 6) (%)	ψ_∞/ψ_{1000h} (−)
GFRP	V1	8	25	1000	2.00	7.163E−03	4.290E−03	0.977	3.29	1.65
	V2				1.76	6.280E−03	3.784E−03	0.970	2.90	1.65
	V3				3.01	3.403E−03	8.915E−03	0.960	5.69	1.89
	V4				3.82	2.508E−03	1.191E−02	0.955	7.39	1.93
	V5				1.55	8.597E−04	4.889E−03	0.971	3.02	1.95
	V6		40		3.81	8.363E−03	9.928E−03	0.992	6.79	1.78
	V7				3.97	2.530E−04	1.313E−02	0.998	7.90	1.99
	V8				2.22	2.748E−03	6.494E−03	0.965	4.17	1.88
	V9	12	20		3.57	1.310E−02	7.521E−03	0.965	5.82	1.63
	V10				2.60	2.511E−04	8.570E−03	0.941	5.17	1.99
BFRP	V11	8	40		3.30	1.329E−02	6.583E−03	0.976	5.28	1.60
	V12				3.96	4.774E−03	1.161E−02	0.979	7.44	1.88
	V13		50		5.82	8.465E−03	1.658E−02	0.992	10.79	1.85
	V14				2.64	1.478E−02	3.884E−03	0.982	3.81	1.44
	V15				4.02	2.076E−02	6.474E−03	0.990	5.96	1.48
	V16	10	40		2.45	9.444E−03	5.012E−03	0.990	3.95	1.61
	V17				3.95	1.331E−02	8.742E−03	0.998	6.58	1.67
	V18		70		3.93	1.485E−02	8.162E−03	0.996	6.38	1.62
GFRP—average				1000	2.83	4.493E−03	7.944E−03	−	5.21	1.84
BFRP—average					3.76	1.246E−02	8.380E−03	−	6.27	1.67

hour-based approaches, it is reasonable to set the required end-of-life time t_∞ at 1,000,000 h ($\approx$114 years).[8] Thus, the prediction of the relaxation rates tends toward the safe side, with the results consciously overestimating the relaxation losses for about 14 years. According to Hull and Clyne,[15] the relaxation intensity decreases over time because the stress redistribution from the matrix to the fibers results in decreased residual stress levels in the matrix, implying a diminished stress redistribution or relaxation intensity. Also, as stated above, the stress redistribution from the matrix to the fibers is the principal reason for the relaxation and is mainly responsible for the observed relaxation characteristics. Therefore, to extrapolate the relaxation rates up to t_∞, Shi et al.,[25] among others, show that it is appropriate to use a logarithmic function like the one in Equation (6).

$$\psi(t) = a_{log} + b_{log} \times \log(t). \quad (6)$$

In Equation (6), the nondimensional relaxation rate is denoted by $\psi(t)$, the time in hours by t and the empirical regression parameters of the logarithmic formula that are individually determined for every test using the least squares method by a_{log} and b_{log}, respectively. Table 4 shows the predicted values of the relaxation rates $\psi(t_\infty)$ using the logarithmic approach according to Equation (6). The numeric approximations show a good agreement between the experimental values and the calculation, which is confirmed by the coefficients of determination R^2. These values are mostly $R^2 \geq 0.95$, where $R^2 = 1$ implies a perfect correlation between the experimental and the calculated values. In general, when comparing the relaxation rate at t_∞ with the relaxation rate at the end of the experiment after 1000 h, a range of $1.44 < \psi_\infty/\psi_{1000h} < 1.99$ can be observed. This allows the conclusion that to calculate relaxation losses within the preliminary dimensioning of prestressed concrete members, the relaxation rate at t_∞ can be predicted with sufficient reliability using $\psi_\infty \approx 2 \times \psi_{1000h}$.

4.4 | Residual tensile properties

After completing the long-term tests, the residual properties of the FRP specimens were determined in the same manner as described in Section 3.2. The observed residual tensile properties (res) and the tensile properties from the preliminary loading phase (pre) are shown in Table 5.

The residual values of the modulus of elasticity indicate that the sustained load does not reduce the stiffness

TABLE 5 Residual and preliminary tensile properties of the tested FRP reinforcement bars.

Reinforcement	Specimen	$\varnothing_{nom}$ (mm)	$\sigma_0/f_{t,m}$ (%)	t_{exp} (h)	E_{pre} (N/mm²)	E_{res} (N/mm²)	E_{res}/E_{pre} (–)	f_{res} (N/mm²)	$f_{res}/f_{t,m}$ (–)	Failure mode
GFRP	V1	8	25	1000	47,318	46,458	0.98	1194	1.03	Tensile rupture of the fibers in the free length
	V2				47,722	46,208	0.97	1130	0.97	
	V3				51,782	51,308	0.99	1192	1.03	
	V4				50,685	50,097	0.99	1133	0.98	
	V5				47,302	47,678	1.01	1135	0.98	
	V6		40		49,500	49,276	1.00	1212	1.04	
	V7				44,825	45,833	1.02	1175	1.01	
	V8				47,678	47,657	1.00	958	0.83	
	V9	12	20		50,290	50,570	1.01	1211	1.01	
	V10				50,061	50,415	1.01	1142	0.96	
BFRP	V11	8	40		43,588	43,500	1.00	962	1.01	
	V12				39,416	39,250	1.00	737	0.77	
	V13		50		42,368	43,557	1.03	945	0.99	
	V14				46,100	46,329	1.00	964	1.01	
	V15				46,150	45,960	1.00	956	1.00	
	V16	10	40		42,296	42,787	1.01	890	0.94	
	V17				43,573	43,625	1.00	989	1.04	
	V18		70		45,935	45,696	0.99	1029	1.08	

of the examined FRP reinforcement throughout the testing period of up to 1000 h and load levels of up to 70% of the tensile strength. The resulting average ratio is $E_{res}/E_{pre} = 1.00$. Therefore, the original assumption derived from the findings of Trost[23] and Shi et al.,[25] that the modulus of elasticity of FRP reinforcement under sustained loads can be taken as constant can be validated based on the available results. A similar behavior can be observed when comparing the residual tensile strength of the specimens with the mean tensile strength of short-term reference tests, see Section 3.3, resulting in an average ratio of $f_{res}/f_{pre} = 0.98$. The two exceptions are specimens V8 and V12 with ratios of $f_{res}/f_{pre} = 0.83$ and $f_{res}/f_{pre} = 0.77$, whose comparably low residual tensile strengths are attributed to damage on the surface of the specimens. In case of V8, the damage occurred during the transfer of the specimen between the long-term and the residual tensile tests. For specimen V12, a production defect was observable, as parts of the bar were not fully impregnated in resin and the surface fibers had been destroyed prior to the residual tensile test.

5 | CONCLUSIONS

The relaxation behavior of GFRP and BFRP reinforcement bars and the determination of their relaxation rates were presented in this paper. It was illustrated that the relaxation process and the creep process are interlinked, enabling the determination of relaxation rates based on the conversion of experimental creep data. This process was substantiated with two different mechanical–mathematical approaches by Trost[24] and Shi et al.[25] It was demonstrated that the approach by Trost with a constant relaxation coefficient $\rho = 0.8$ is valid for the determination of time-dependent properties of FRP reinforcement bars.

The investigation of the time-dependent material properties of two types of FRP reinforcement (GFRP reinforcement bars with $\varnothing_{nom} = 8$ and 12 mm and BFRP reinforcement bars with $\varnothing_{nom} = 8$ and 10 mm) was based on long-term tensile tests under sustained load within a load-magnifying steel frame. The resulting relaxation rates for sustained load levels of $0.2 < \sigma_0/f_{t,m} < 0.7$ and a test period of 1000 h ranged from $\psi_{1000h} = 1.76\%$ to $\psi_{1000h} = 5.82\%$.

The experimental results were extrapolated using a logarithmic function to determine the relaxation rates at the end of a concrete members' service life. The resulting relaxation rates are within a range of $1.44 < \psi_\infty/\psi_{1000h} < 1.99$, indicating that the relaxation rates at t_∞ can be conservatively estimated with $\psi_\infty \approx 2 \times \psi_{1000h}$ for the preliminary calculation of prestress losses.

After completion of the long-term tests, the residual tensile properties of the FRP reinforcement bars were

determined with the results allowing the assumption that sustained loads with load levels of up to $\sigma_0/f_{t,m} = 0.70$ and a duration of up to 1000 h do not negatively influence the mechanical properties of the investigated FRP reinforcement bars.

ACKNOWLEDGMENTS

CONFLICT OF INTEREST STATEMENT

The authors declare no conflict of interest.

DATA AVAILABILITY STATEMENT

Research data are not shared.

ORCID

Dominik Hiesch 🅾 https://orcid.org/0000-0002-3712-1952
Redouan El Ghadioui 🅾 https://orcid.org/0000-0002-4523-0075

REFERENCES

1. Angst U, Elsener B, Jamali A, Adey B. Concrete cover cracking owing to reinforcement corrosion—theoretical considerations and practical experience. Mater Corros. 2012;63(12):1069–77.
2. El Ghadioui R, Proske T, Tran NL, Graubner C-A. Structural behaviour of CFRP reinforced concrete members under bending and shear loads. Mater Struct. 2020;53(3):63.
3. Schumann A, May M, Curbach M. Carbonstäbe im Bauwesen: Teil 1: Grundlegende Materialcharakteristiken, English title: Rebars made of carbon fibres for the use in civil engineering: part 1: fundamental material characteristics. Beton- Stahlbetonbau. 2018;113(12):868–76.
4. Hofmann S, Tran NL, Proske T, Graubner C-A. Shear capacity of BFRP reinforced concrete beams without shear reinforcement. In: Zingoni A, editor. Advances in engineering materials, structures and systems: innovations, mechanics and applications. London: CRC Press; 2019. p. 1531–6.
5. Wolf B, Glomb DS, Kustermann A, Dauberschmidt C. Untersuchung des Zug- und Verbundverhaltens von Basaltfaserverstärkter Kunststoff-Stabbewehrung in Beton, English title: investigation on tension and bonding behaviour of basalt fibre reinforced polymers in concrete structures. Beton- Stahlbetonbau. 2019;114(7):454–64.
6. Knab F, Weber A, Schweinfurth J. Sicherer Einsatz von Glasfaserbewehrung im Bauwesen, English title: safe application of glass fibre rebar in civil engineering - hints and examples for practice. Beton- Stahlbetonbau. 2015;110(12):822–31.
7. Benmokrane B, Brown VL, Mohamed K, Nanni A, Rossini M, Shield C. Creep-rupture limit for GFRP bars subjected to sustained loads. J Compos Constr. 2019;23(6):06019001.
8. International Federation for Structural Concrete. FRP reinforcement in RC structures. Lausanne: International Federation for Structural Concrete (*fib*); 2007.
9. ACI 440.1R-15. Guide for the design and construction of structural concrete reinforced with fiber-reinforced polymer (FRP) bars. Farmington Hills, MI: American Concrete Institute; 2015.
10. Nanni A, de Luca A, Zadeh HJ. Reinforced concrete with FRP bars: mechanics and design. 1st ed. Boca Raton, FL: Taylor & Francis Group; 2014.
11. Rossini M. FRP reinforcement for prestressed concrete applications [dissertation]. Coral Gables, FL: University of Miami; 2019.
12. Inman M, Thorhallsson ER, Azrague K. A mechanical and environmental assessment and comparison of basalt fibre reinforced polymer (BFRP) rebar and steel rebar in concrete beams. Energy Procedia. 2017;111:31–40.
13. Przygocka M, Kotynia R. Pre-stress losses in FRP pre-stressed reinforced concrete—subject overview. Arch Civ Eng. 2018; 64(4):257–68.
14. Ehrenstein GW. Faserverbund-Kunststoffe: Werkstoffe - Verarbeitung - Eigenschaften. 2. völlig überarbeitete Auflage. München/Wien: Carl Hanser Verlag; 2006.
15. Hull D, Clyne TW. An introduction to composite materials. 2nd ed. Cambridge: Cambridge University Press; 1996.
16. ACI 440.4R-04. Prestressing concrete structures with FRP tendons. Farmington Hills: American Concrete Institute; 2004.
17. Dolan CW, Hamilton HR, Bakis CE, Nanni A. Design recommendations for concrete structures prestressed with FRP tendons; DTFH61-96-C-00019. U. S. Department of Transportation, Federal Highway AdministrationWashington, DC; 2001.
18. Youssef T, Benmokrane B. Creep behaviour and residual tensile properties of GFRP reinforcing bars subjected to different sustained service loads. ACI Spec Publ. 2011;275:39.1–39.20.
19. Ascione L, Berardi VP, D'Aponte A. Creep phenomena in FRP materials. Mech Res Commun. 2012;43:15–21.
20. fib Bulletin 40. FRP reinforcement in RC structures. Lausanne: Fédération internationale du béton; 2007.
21. CSA S6-14. Canadian highway bridge design code. Mississauga: Canadian Standards Association CSA; 2014.
22. DIN EN 1990. Eurocode: Grundlagen der Tragwerksplanung; deutsche Fassung EN 1990:2002 + A1:2005 + A1:2005/AC: 2010, English title: Eurocode: basis of structural design; German version EN 1990:2002 + A1:2005 + A1:2005/AC:2010 [DIN Deutsches Institut für Normung e. V.]. Berlin: Beuth Verlag; 2010.
23. Trost H. Auswirkungen des Superpositionsprinzips auf Kriech- und Relaxationsprobleme bei Beton und Spannbeton, English title: effects of the principle of superposition on creep and relaxation problems in concrete and prestressed concrete. Beton- Stahlbetonbau. 1967;1967(10/11):230–8.
24. Trost H. Dischingers grundlegende Arbeiten und neuere Erkenntnisse über die Auswirkungen zeitabhängigen Werkstoffverhaltens in vorgespannten und nicht-vorgespannten Stahlbetonkonstruktionen. In: Specht M, editor. Spannweite der Gedanken - Zur 100. Wiederkehr des Geburtstages von Franz Dischinger. Berlin: Springer-Verlag; 1987. p. 213–26.
25. Shi J, Wang X, Huang H, Wu Z. Relaxation behavior of prestressing basalt fiber-reinforced polymer tendons considering anchorage slippage. J Compos Mater. 2017;51(9):1275–84.
26. Wang X, Shi J, Liu J, Yang L, Wu Z. Creep behavior of basalt fiber reinforced polymer tendons for prestressing application. Mater Des. 2014;59:558–64.

27. Sayed-Ahmed M, Hajimiragha B, Hajimiragha B, Mohamed K, Benmokrane B. Creep rupture and creep behaviour of newly third generation GFRP bars subjected to sustained loads. CDCC 2017 Fifth International Conference on Durability of FRP Composites for Construction and Rehabilitation of Structures 2017.

28. Yang D, Zhang J, Song S, Zhou F, Wang C. Experimental investigation on the creep property of carbon fiber reinforced polymer tendons under high stress levels. Materials. 2018;11(11): 2273.

29. ASTM D7205/D7205M-06. Test method for tensile properties of fiber reinforced polymer matrix composite bars. West Conshohocken, PA: ASTM International; 2006.

30. ISIS Canada Corporation. ISIS Design Manual No. 5: Prestressing concrete structures with fibre-reinforced polymers [ISIS Canada Research Network]. Winnipeg: ISIS Canada Corporation; 2008.

31. Rossini M, Saqan E, Nanni A. Prediction of the creep rupture strength of GFRP bars. Construct Build Mater. 2019;227: 116620.

32. ACI 440.3R-12. Guide test methods for fiber-reinforced polymers (FRPs) for reinforcing or strengthening concrete and masonry structures. Farmington Hills: American Concrete Institute; 2012.

33. Park S-J. Carbon fibers. Vol 210. Singapore: Springer Singapore; 2018.

AUTHOR BIOGRAPHIES

Dominik Hiesch, TU Darmstadt, Institute of Concrete and Masonry Structures, Darmstadt, Germany.

Tilo Proske, TU Darmstadt, Institute of Concrete and Masonry Structures, Darmstadt, Germany.

Carl-Alexander Graubner, TU Darmstadt, Institute of Concrete and Masonry Structures, Darmstadt, Germany.

Lukas Bujotzek, TU Darmstadt, Institute of Concrete and Masonry Structures, Darmstadt, Germany.

Redouan El Ghadioui, TU Darmstadt, Institute of Concrete and Masonry Structures, Darmstadt, Germany.